OBSCURED AGNs IN BULGELESS HOSTS DISCOVERED BY WISE : THE CASE STUDY OF SDSS J1224+5555

The Astrophysical Journal, 827:58 (12pp), 2016 August 10 doi:10.3847/0004-637X/827/1/58

OBSCURED AGNs IN BULGELESS HOSTS DISCOVERED BY *WISE*: THE CASE STUDY OF SDSS J1224+5555

S. Satyapal[1,2], N. J. Secrest[1,3,8], B. Rothberg[1,4], J. A. O'Connor[1], S. L. Ellison[5], R. C. Hickox[6], A. Constantin[7], M. Gliozzi[1], and and J. L. Rosenberg[1]

[1] George Mason University, Department of Physics & Astronomy, MS 3F3, 4400 University Drive, Fairfax, VA 22030, USA
[2] Department of Astronomy, University of Maryland, College Park, MD 20742, USA
[3] United States Naval Observatory, Washington, DC 20392, USA
[4] LBT Observatory, University of Arizona, 933 N. Cherry Ave., Tuscan, AZ 85721, USA
[5] Department of Physics and Astronomy, University of Victoria, Victoria, BC V8P 1A1, Canada
[6] Department of Physics and Astronomy, Dartmouth College, 6127 Wilder Laboratory, Hanover, NH 03755, USA
[7] Department of Physics and Astronomy, James Madison University, Harrisonburg, VA 22807, USA
Received 2016 March 28; revised 2016 May 29; accepted 2016 June 2; published 2016 August 8

ABSTRACT

There is mounting evidence that supermassive black holes (SMBHs) form and grow in bulgeless galaxies. However, a robust determination of the fraction of active galactic nuclei (AGNs) in bulgeless galaxies, an important constraint to models of SMBH seed formation and merger-free models of AGN fueling, is unknown, since optical studies have been shown to be incomplete for AGNs in low-mass galaxies. In a recent study using the *Wide-field Infrared Survey Explorer*, we discovered hundreds of bulgeless galaxies that display mid-infrared signatures of extremely hot dust suggestive of powerful accreting massive black holes, despite having no signatures of black hole activity at optical wavelengths. Here we report X-ray follow-up observations of J122434.66+555522.3, a nearby ($z = 0.052$) isolated bulgeless galaxy that contains an unresolved X-ray source detected at the 3σ level by *XMM-Newton* with an observed luminosity uncorrected for intrinsic absorption of $L_{2-10\,\mathrm{keV}} = (1.1 \pm 0.4) \times 10^{40}\,\mathrm{erg\,s^{-1}}$. Ground-based near-infrared spectroscopy with the Large Binocular Telescope and multiwavelength observations from ultraviolet to millimeter wavelengths together suggest that J1224+5555 harbors a highly absorbed AGN with an intrinsic absorption of $N_{\mathrm{H}} > 10^{24}\,\mathrm{cm^{-2}}$. The hard X-ray luminosity of the putative AGN corrected for absorption is $L_{2-10\,\mathrm{keV}} \sim 3 \times 10^{42}\,\mathrm{erg\,s^{-1}}$, which, depending on the bolometric correction factor, corresponds to a bolometric luminosity of the AGN of L_{bol}. $\sim 6 \times 10^{43}$–$3 \times 10^{44}\,\mathrm{erg\,s^{-1}}$ and a lower mass limit for the black hole of $M_{\mathrm{BH}} \simeq 2 \times 10^{6}\ M_{\odot}$, based on the Eddington limit. While enhanced X-ray emission and hot dust can be produced by star formation in extremely low metallicity environments typical in dwarf galaxies, J1224+5555 has a stellar mass of $\sim 2.0 \times 10^{10}\ M_{\odot}$ and an above solar metallicity ($12 + \log \mathrm{O/H} = 9.11$), typical of our *WISE*-selected bulgeless galaxy sample. While collectively these observations suggest the presence of an AGN, we caution that identifying obscured AGNs in the low-luminosity regime is challenging and often requires multiwavelength observations. These observations suggest that low-luminosity AGNs can be heavily obscured and reside in optically quiescent galaxies, adding to the growing body of evidence that the fraction of bulgeless galaxies with accreting black holes may be significantly underestimated based on optical studies.

Key words: galaxies: active – galaxies: bulges – X-rays: galaxies

1. INTRODUCTION

Over 40 supermassive black holes (SMBHs) with masses $\sim 10^{9}\ M_{\odot}$ have been discovered at $z > 6$, including one with $\sim 10^{10}\ M_{\odot}$ (e.g., Fan et al. 2006; Mortlock et al. 2011; Venemans et al. 2013; Wu et al. 2015). The existence of such massive black holes when the universe was less than 1 billion yr old poses significant challenges to theories of the origin of SMBH seeds and their subsequent growth. The seed population could have formed from the remnants of primordial stars (e.g., Volonteri et al. 2003; Volonteri & Rees 2005; Johnson & Bromm 2007), which would create the lowest-mass seeds ($\sim 10^{2}\ M_{\odot}$), or in dense star clusters through runaway stellar mergers (e.g., Begelman & Rees 1978; Ebisuzaki et al. 2001), which would create intermediate-mass seeds ($\sim 10^{4}\ M_{\odot}$), or from the direct collapse of self-gravitating pre-galactic gas disks at high redshifts in cooling halos (e.g., Haehnelt & Rees 1993; Bromm & Loeb 2003; Agarwal et al. 2014), which would produce the most massive seeds ($\sim 10^{4}$–$10^{6}\ M_{\odot}$) (see review by Natarajan 2014). While the lowest-mass seeds are the easiest to form, early continuous and extremely efficient growth of the seeds required for the production of massive quasars at $z > 6$ poses significant challenges, a problem that is exacerbated by recent simulations of early star formation that show that the progenitor Population III stars may be even less massive than initially thought due to turbulence and efficient fragmentation that inhibits the growth of massive stars (e.g., Alvarez et al. 2009; Greif et al. 2011; Regan et al. 2014; Safranek-Shrader et al. 2014). Discriminating between these various seed formation mechanisms is challenging, since seed formation occurs at redshifts $z > 15$ and is therefore observationally inaccessible. However, as pointed out by several recent studies (e.g., Volonteri & Natarajan 2009; van Wassenhove et al. 2010; Volonteri 2010; Greene 2012), the occupation fraction and mass function of nuclear black holes in local low-mass galaxies and galaxies that lack classical bulges can provide important constraints on the original seed population, since these galaxies have presumably had a quiescent cosmic history and therefore their black holes carry the imprint of the original seed population. Apart from providing constraints on models of the origins of SMBHs, the search for active galactic

[8] National Research Council Postdoctoral Fellow.

nuclei (AGNs) in the small bulge mass regime is of intrinsic interest, since it is required in order to obtain a complete census of AGN activity in the local universe. Furthermore, the mass and accretion rates of these SMBHs provide insight into our understanding of the efficiency of secular processes in the growth of nuclear black holes (e.g., Hopkins et al. 2014). As a result, the search for black holes in the low bulge mass regime has been an area of active research over the past decade.

In recent years, there have been a number of discoveries of AGNs in low-mass galaxies or galaxies that lack classical bulges, suggesting that black holes do exist in the low bulge mass regime and are more common than previously thought (e.g., Filippenko & Ho 2000; Barth et al. 2004; Greene & Ho 2007; Satyapal et al. 2007, 2008, 2009, 2014; Dewangan et al. 2008; Ghosh et al. 2008; Izotov & Thuan 2008; Shields et al. 2008; Desroches & Ho 2009; Gliozzi et al. 2009; Araya Salvo et al. 2010; McAlpine et al. 2010; Jiang et al. 2011; Reines et al. 2011, 2013, 2014; Dong et al. 2012; Ho et al. 2012; Reines & Deller 2012; Secrest et al. 2012, 2013, 2015b; Coelho et al. 2013; Schramm et al. 2013; Simmons et al. 2013; Bizzocchi et al. 2014; Maksym et al. 2014; Moran et al. 2014; Yuan et al. 2014; Graham & Scott 2015; Lemons et al. 2015; Miller et al. 2015; Sartori et al. 2015; Graham et al. 2016; Mezcua et al. 2016). However, despite the recent advent of the vast amount of optical spectroscopic data available from the Sloan Digital Sky Survey, to date, there still exist only small samples of AGNs discovered by optical surveys in small-bulge galaxies and only a handful with no evidence for any bulge. Indeed, a key and striking result based on optical spectroscopic studies is that the fraction of galaxies with signs of accretion activity drops dramatically at stellar masses $\log M_\star/M_\odot < 10$ (e.g., Kauffmann et al. 2003). For a sample of dwarf galaxies with stellar masses $\log M_\star/M_\odot < 9.5$ and high-quality optical emission line measurements, only 0.1% of galaxies are unambiguously identified as AGNs based on their optical line ratios (Reines et al. 2013).

Using the all-sky *Wide-Field Infrared Sky Explorer Survey* (*WISE*; Wright et al. 2010), we discovered several hundred optically normal bulgeless galaxies that display red mid-infrared colors [3.4 μm]–[4.6 μm] (hereafter *W*1–*W*2) suggestive of dominant AGNs (Stern et al. 2012) that may outnumber optically identified AGNs by as much as a factor of ≈6 (Satyapal et al. 2014). Most of these galaxies do not show signatures of AGNs in their optical emission line ratios, suggesting heavy obscuration or dilution of emission-line ratios by vigorous star formation, both of which are well-known limitations to optical spectroscopic surveys in finding low-luminosity AGNs (e.g., Goulding & Alexander 2009; Hopkins et al. 2009; Trump et al. 2015; Pons & Watson 2014).

While the red mid-IR colors discovered by *WISE* are highly suggestive of accretion activity, it is possible that the dust can be heated by star formation alone, and there are a number of blue compact dwarfs (BCDs) where this is indeed taking place (e.g., Griffith et al. 2011; Izotov et al. 2014). On the other hand, if the majority of bulgeless galaxies that display red mid-infrared colors are in fact AGNs, the fraction of AGNs in the low bulge mass regime has been significantly underestimated by optical studies.

In a pilot study using *XMM-Newton*, we obtained follow-up X-ray observations of two bulgeless galaxies with red *WISE* colors in order to confirm the AGN. In Secrest et al. (2015b), we presented the *XMM-Newton* observation of the bulgeless galaxy SDSS J132932.41+323417.0, a blue, irregular dwarf galaxy ($\log M_\star/M_\odot = 8.3$) with a metallicity of $Z/Z_\odot = 0.4$, at a redshift of $z = 0.0156$, which contains a hard, unresolved X-ray source detected by *XMM-Newton* with luminosity $L_{2\text{–}10\ \mathrm{keV}} = 2.4\times10^{40}\,\mathrm{erg\ s^{-1}}$, over two orders of magnitude greater than that expected from star formation, providing convincing evidence for the presence of an accreting massive (10^4–$10^5\ M_\odot$) black hole.

In this paper, we present the *XMM-Newton* observations of the nearby ($z = 0.052$) isolated bulgeless galaxy SDSS J122434.66+555522.3 (hereafter J1224+5555), together with ground-based near-infrared spectra obtained with the Large Binocular Telescope (LBT). Unlike SDSS J132932.41+323417.0 (hereafter J1329+3234), J1224+5555 is not a dwarf galaxy. It has a mass of $\log M_\star/M_\odot = 10.3$, comparable to the mean mass of the bulgeless sample presented in Table 1 of Satyapal et al. (2014), and a metallicity that is above solar (12 + logO/H = 9.11), based on Tremonti et al. (2004). J1224+5555 hosts an unresolved mid-infrared nuclear source with extremely red colors typical of powerful AGNs (*W*1–*W*2 = 1.102 mag; *W*2–*W*3 = 3.564 mag) based on the final *WISE* all-sky data release catalog (AllWISE[9]). Based on the optical emission line ratios from the Sloan Digital Sky Survey (SDSS) spectrum, there is no evidence for an AGN based on either the Kewley et al. (2001) or the Kauffmann et al. (2003) diagnostics ($\log([\mathrm{O\ III}]_{\lambda5007}/\mathrm{H}\beta) = -0.75$, $\log([\mathrm{N\ II}]_{\lambda6584}/\mathrm{H}\alpha) = -0.39$). In Section 2, we describe our X-ray and near-infrared ground-based observations and data analysis, followed by a description of our results in Section 3. In Sections 4–6, we discuss various possible explanations for the origin of the X-ray, mid-infrared, and near-infrared emission in J1224+5555, including obscured star formation and a deeply embedded AGN. In Section 7, we analyze the multiwavelength spectral energy distribution (SED) of J1224+5555. In Section 8, we discuss the implications of our results, and we summarize our findings in Section 9.

We adopt a standard ΛCDM cosmology with $H_0 = 70$ km s^{-1} Mpc^{-1}, $\Omega_\mathrm{M} = 0.3$, and $\Omega_\Lambda = 0.7$.

2. OBSERVATIONS AND DATA REDUCTION

2.1. XMM *Observations*

J1224+5555 was observed for 10 ks twice by *XMM-Newton*, on 2013 May 9 (obsid = 0721900401) and 2013 May 11 (obsid = 0721900601), as part of a pilot follow-up study (Cycle 12 GO, prop. 072190) using *XMM-Newton* to investigate the nature of the red *WISE* sources presented in Satyapal et al. (2014). We note that a total of four targets were observed in this program. One of the targets (SDSS J012218.11+010025.8) was a merging system for which we obtained follow-up *Chandra* observations. The *XMM* and *Chandra* observations of this target will be published as a larger sample of X-ray-identified dual AGNs (S. Satyapal et al. 2016, in preparation). The fourth target was observed with *XMM-Newton* (SDSS J082240.29+034546.5), but the *WISE* photometry from the ALLWISE release of the *WISE* catalog showed that the magnitudes from the previous release were erroneous, and the source actually does not have updated red colors that meet the AGN criteria adopted in Satyapal et al. (2014). The

[9] wise2.ipac.caltech.edu/docs/release/allwise/

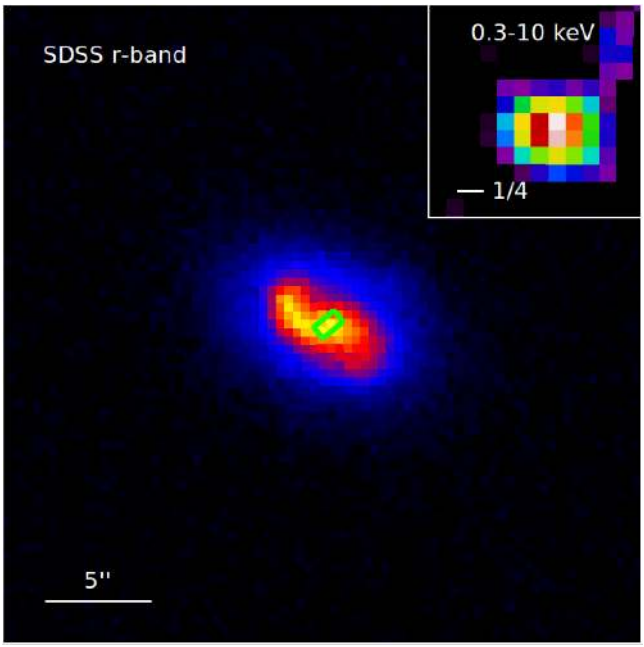

Figure 1. SDSS *r*-band image with insert of 0.3–10 keV X-ray image at 1/4 scale. X-ray image binned by 64 and smoothed with a 3 pixel Gaussian for clarity. The LUCI-1 extraction aperture is overlaid in green.

observations presented here are thus the second of only two isolated bulgeless galaxies from the sample from Satyapal et al. (2014) for which follow-up X-ray observations were obtained.

We reduced the data with the *XMM-Newton Science Analysis Software*, version 13.0.0, using the most up-to-date calibration files. We filtered our event files using `evselect` for "good" (`FLAG` = 0). Examination of the pn data reveals a faint source associated with J1224+5555 (see Figure 1). To obtain better photon statistics, we merged the (cleaned) event files from all cameras and both observations into a single event file using the `merge` task. We created a 0.3–10 keV image of J1224+5555, binned by a factor of 64, and we used `eregionanalyse` to extract counts and compute the background-subtracted count rate for the X-ray source. We used a circular extraction region centered on J1224+5555 with a radius of 200 pixels (10″), which we found to be the optimum extraction radius for maximizing the signal-to-noise ratio (S/N). The encircled energy factor for this extraction region is 0.62. We used a 1200 pixel (1′) radius background region, which we placed on a neighboring, source-free area on the image.

We used a weighted Galactic total hydrogen column density of $N_{\rm H} = 1.20 \times 10^{20}\,{\rm cm}^{-2}$, derived from the *Swift* Galactic $N_{\rm H}$ tool,[10] which is based on the work of Willingale et al. (2013) that appends the molecular hydrogen column density $N_{\rm H\,II}$ to the atomic hydrogen column density $N_{\rm H\,I}$ from the Leiden/Argentine/Bonn (LAB) 21 cm survey (Kalberla et al. 2005).

2.2. LBT Observations

In order to search for obscured star formation, or broad lines obscured in the optical, we obtained near-infrared ground-based spectroscopy with the LBT NIR Spectroscopic Utility with Camera Instruments (LUCI-1) instrument (Seifert et al. 2003, 2010) mounted on the left bent Gregorian focus of the Large Binocular Telescope (LBT) on 2015 March 28. The LBT employs two 8.4 m mirrors on a single mount. LUCI-1 is a near-IR imager/spectrograph for the LBT with wavelength coverage of 0.85–2.4 μm (*zJHK* bands) in imaging, long-slit, and multi-object spectroscopy modes. The spectrum of SDSS J1224+5555 was taken with the N1.8 camera, centered on the coordinates R.A. = $12^{\rm h}24^{\rm m}34\overset{\rm s}{.}64$, decl. = +55°55′22″.619 and a position angle of 40°. We employed a 1″.0 wide × 3″.9 long slit and the G200 grating with the HKspec filter. At the distance of J1224+5555, 1″.0 corresponds to ≈1 kpc. Using calibration Ne and Ar arc lines, we measure an average spectral resolution of 0.0017 μm per pixel, or $R \sim 858$–1376 over this wavelength range. The total integration time was 30 minutes, split into six individual exposures. As the target galaxy is significantly smaller than the slit length, observations were done using an `AB` pattern of nodding along the slit. Thus, every exposure contains the science target. The A0V-type star HIP 56736 was observed before the target at similar airmass, to remove telluric features.

The LUCI-1 data were reduced using a set of custom `IRAF` scripts. Briefly, first the science and A0V telluric star exposures were trimmed and flat-fielded; then, science and telluric star exposures closest in time were pair-subtracted to remove background IR flux and night-sky emission lines. Next, wavelength calibration was done by fitting a third-order *spline3* polynomial to 37 night-sky lines identified in the science exposures. The fitting yielded an rms = 7.68×10^{-5} μm over the entire wavelengh range. In the detector *X*–*Y* pixel reference frame LUCI-1 spectra are slightly tilted along the *X*-axis and show non-negligible curvature in the *Y*-direction. To correct for both of these effects, the `IRAF` tasks `REID`, `FITC`, and `TRANSFORM` were used to straighten and rectify all science and A0V telluric star exposures via the wavelength calibration applied to the central five rows. The pair-subtracted science frames were then shifted in *Y* and combined into a single frame in order to improve the S/N for extracting a one-dimensional spectrum. The `IRAF` task `APALL` was used to extract a one-dimensional spectrum using a 2 pixel (or 0″.5 in angular size) diameter aperture from the combined science frame. At the redshift of the target, 2 pixels corresponds to an aperture of 500 pc. The angular size of the aperture was chosen based on the measured FWHM of stars in the acquisition images, the FWHM in the spatial direction of the telluric star frames, and continual monitoring of the wavefront sensor of the guide camera.

Once the one-dimensional, wavelength-calibrated science and telluric spectra were extracted, corrections and flux calibration were applied using the `IDL`-based software `XTELLCOR GENERAL`. This package uses the spectrum of an A0V star observed close in time and airmass to the science target and a high-resolution spectrum model of Vega to create a telluric correction spectrum free of stellar absorption lines in order to then remove telluric absorption features in the data (Vacca et al. 2003). `XTELLCOR GENERAL` also flux-calibrates the science data using the known $(B - V)$ color of the A0V star, and assuming that there are not significant slit losses in the observations. The final telluric-corrected and flux-calibrated data were then used for analysis in the paper.

[10] http://www.swift.ac.uk/analysis/nhtot/index.php

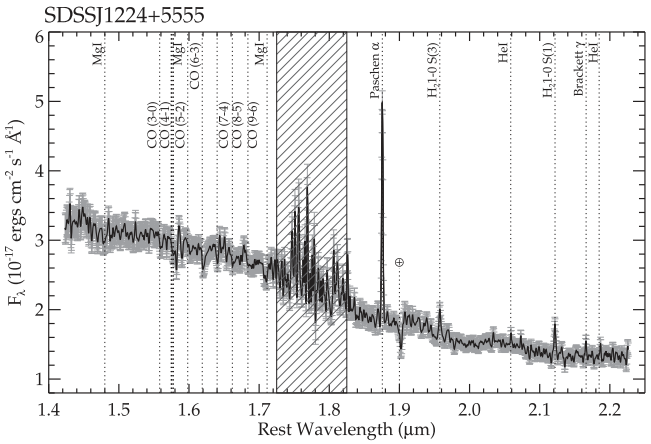

Figure 2. LBT LUCI-1 near-infrared spectrum of the nuclear source corrected for redshift, with labels for features detected. Also noted is a strong telluric absorption feature at 1.9 μm from imperfect telluric corrections, indicated by the encircled plus line. The diagonally hatched lines note a region of strong absorption due to Earth's atmosphere.

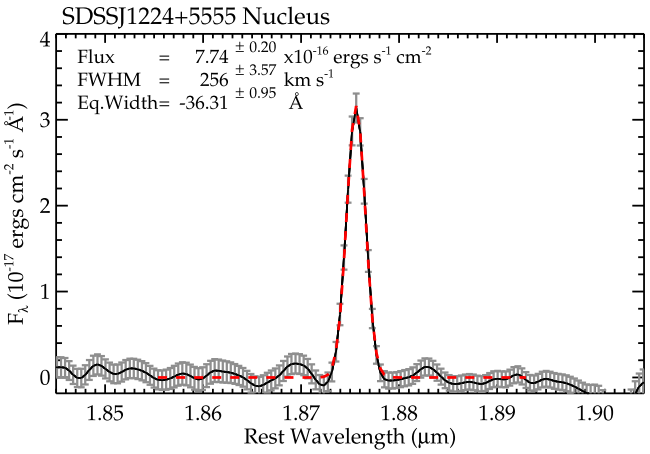

Figure 3. Near-infrared spectrum centered on the Paα line. The red line denotes the fit to the Paα line, while the gray denotes the rms noise.

3. RESULTS

3.1. X-Ray Results

Using the source and background extraction regions described in Section 2.1, we find 25 ± 8 counts in the range 0.3–10 keV for J1224+5555, a 3σ detection. The effective exposure time for the merged event file was 20 ks, yielding a background-subtracted count rate of $(1.2 \pm 0.4) \times 10^{-3}$ counts s^{-1}. Because we do not have enough counts to reliably estimate a hardness ratio, we estimated hard (2–10 keV) X-ray fluxes assuming a typical AGN power-law X-ray spectrum with index $\Gamma = 1.8$ and using WebPIMMS.[11] The observed hard X-ray luminosity (assuming no intrinsic absorption) is $L_{2-10\,\mathrm{keV}} = (1.1 \pm 0.4) \times 10^{40}$ erg s^{-1}. If we assume a value for the intrinsic absorption of $N_{\mathrm{H}} = 10^{21}$ cm^{-2}, we estimate an unabsorbed hard X-ray luminosity of $L_{2-10\,\mathrm{keV}} = (1.6 \pm 0.5) \times 10^{40}$ erg s^{-1}. If this source is nearly Compton thick ($N_{\mathrm{H}} \approx 10^{24}$ cm^{-2}; see Section 5), the unabsorbed hard X-ray luminosity is $L_{2-10\,\mathrm{keV}} \sim 3 \times 10^{42}$ erg s^{-1}. We note that the X-ray data alone are not sufficient to constrain the column density.

3.2. Near-infrared Spectrum

In Figure 2, we plot the 1D near-infrared spectrum corresponding to the position of the near-IR unresolved nuclear source. We detect a prominent Paα line at $\lambda = 1.876$ μm. The near-infrared spectrum centered on the Paα line is shown in Figure 3. The total Paα flux within the 0.″5 aperture is $F_{\mathrm{Pa}\alpha} = (7.74 \pm 0.20) \times 10^{-16}$ erg cm^{-2} s^{-1} with an FWHM, corrected for the instrumental resolution, of 256 ± 3.57 km s^{-1}. There is no evidence for any broad component to the emission line, and no high-excitation lines were detected. We report approximately 3σ detections of the $H_2\,1-0S(3)$ 1.957 μm and $H_2\,1-0S(3)$ 2.121 μm with fluxes of $(1.37 \pm 0.39) \times 10^{-16}$ erg cm^{-2} s^{-1} and $(1.26 \pm 0.29) \times 10^{-16}$ erg cm^{-2} s^{-1}, respectively. The 3σ upper limit to the [Fe II] 1.644 μm flux is $F_{[\mathrm{Fe\,II}]} \lesssim 6.27 \times 10^{-17}$ erg cm^{-2} s^{-1}. The 3σ upper limit to the Brγ flux is $F_{\mathrm{Br}\gamma} \lesssim 9.32 \times 10^{-17}$ erg cm^{-2} s^{-1}.

[11] https://heasarc.gsfc.nasa.gov/cgi-bin/Tools/w3pimms/w3pimms.pl

4. THE ORIGIN OF THE X-RAY EMISSION IN J1224+5555

The derived observed X-ray luminosity (uncorrected for intrinsic absorption) of J1224+5555 of $L_{2-10\,\mathrm{keV}} = (1.1 \pm 0.4) \times 10^{40}$ erg s^{-1} is low compared to that of powerful AGNs, and there are insufficient counts to fit the X-ray spectrum and constrain the intrinsic absorption and the nature of the nuclear X-ray source. This leaves open the possibility that the X-ray emission results from the integrated emission from a population of X-ray binaries (XRBs). We explored this possibility by estimating the contribution of XRBs to the observed X-ray emission using the star formation rate (SFR) expected from a similar aperture. The global galaxy-wide SFR from the Max Planck Institut fur Astrophysik/Johns Hopkins University (MPA/JHU) collaboration,[12] which follows Brinchmann et al. (2004) with photometric corrections from Salim et al. (2007), is 2.6 $M_{\odot}$ yr^{-1}. However, since J1224+5555 is a late-type galaxy, it is possible that there is significant extinction at optical wavelengths and that the SFR based on the Hα luminosity is significantly underestimated. We explored this possibility using the observed Paα line flux from the LUCI-1 spectrum. The Hα flux from the MPA catalog for J1224+5555 is $F_{\mathrm{H}\alpha} = (7.735 \pm 0.0797) \times 10^{-15}$ erg cm^{-2} s^{-1}. Since the SDSS Hα flux corresponds to a 3″ circular aperture, larger than the 1.″0 × 0.″5 extraction aperture of the LUCI-1 spectrum, we can get a rough estimate of the extinction toward the recombination line emission by scaling the fluxes assuming a uniform surface brightness. Scaling by the ratio of aperture areas, the aperture-corrected observed Hα-to-Paα line flux ratio for J1224+5555 is 0.70. Assuming an intrinsic ratio of 7.82 for galaxies with $12 + \log(\mathrm{O/H}) > 8.35$ (Osterbrock & Ferland 2006) and adopting an extinction curve with differential reddening of $k(\mathrm{H}\alpha)$–$k(\mathrm{Pa}\alpha) = 2.08$ (Landini et al. 1984), we obtain a color excess of $E(B-V)$ of 1.255.[13] Assuming a Milky-Way-like extinction curve ($R_V = 3.1$), we calculate only a moderate extinction of A_V of 3.89 toward the ionized gas. Since the 1.″0 slit width corresponds to ≈1 kpc at the distance of J1224+5555, it is likely that the bulk of the ionized gas emission is contained

[12] www.mpa-garching.mpg.de/SDSS/

[13] The color excess is calculated using the formula $F_{\mathrm{int}}(\mathrm{H}\alpha)/F_{\mathrm{int}}(\mathrm{Pa}\alpha) = F_{\mathrm{int}}(\mathrm{H}\alpha)/F_{\mathrm{int}}(\mathrm{Pa}\alpha)\,10^{-0.4(k(\mathrm{H}\alpha)-k(\mathrm{Pa}\alpha))E(B-V)}$.

within the LUCI-1 aperture. The aperture correction used above therefore is likely to significantly underestimate the Hα flux in the 1.″0 slit. The extinction is therefore likely to be lower than the value calculated here.

If we use the upper limit to the Brγ flux, we can estimate an upper limit to the extinction. Assuming an intrinsic Paα-to-Brγ flux ratio of 12.5 (Osterbrock & Ferland 2006), the observed line flux ratio corresponds to an $A_V < 5.5$. Thus, the recombination line fluxes detected from J1224+5555 together imply that the extinction toward the nuclear star-forming regions is not excessively large. Indeed, the SFR derived using the far-infrared μm luminosity, a widely used indicator of the unobscured SFR in both star-forming galaxies and AGNs, adopting the value from the recent catalog by Ellison et al. (2016), is $\sim 2.5\ M_\odot\ \mathrm{yr}^{-1}$, in excellent agreement with the MPA value, strongly suggesting that there is no significant embedded star formation in J1224+5555. Thus, both the near-infrared spectra and the far-infrared *IRAS* photometry suggest only moderate extinction toward the star-forming region in J1224+5555. We note that J1224+5555 is not detected at 1.4 GHz by the NRAO VLA Sky Survey[14] or Faint Images of the Radio Sky at Twenty-Centimeters[15] survey. The SFR implied by the upper limit (Bell 2003) of the 1.4 GHz flux is $<7.2\ M_\odot\ \mathrm{yr}^{-1}$, fully consistent with the MPA value, strongly suggesting that there is no significant deeply embedded star formation in J1224+5555.

To calculate the predicted X-ray emission from XRBs, we used the relationship between stellar mass, SFR, and X-ray emission given in Lehmer et al. (2010). Given $\log M_\star/M_\odot = 10.3$ and SFR $= 2.5\ M_\odot\ \mathrm{yr}^{-1}$, the predicted 2–10 keV luminosity due to XRBs is $5.9 \times 10^{39}\ \mathrm{erg\ s}^{-1}$, a factor of ~3 times lower than the apparent X-ray luminosity of J1224+5555 of $L_{2-10\,\mathrm{keV}} = (1.6 \pm 0.5) \times 10^{40}\ \mathrm{erg\ s}^{-1}$. However, there is a considerable scatter on the Lehmer et al. (2010) relation (0.34 dex), indicating that the observed X-ray luminosity is not significantly above the scatter of the relation.

To further explore the possibility that the X-ray emission is of stellar origin, we investigated the age of the nuclear stellar population to determine whether it was consistent with the existence of a large population of XRBs. The relative number of low-mass X-ray binaries (LMXBs) and high-mass X-ray binaries (HMXBs) in a galaxy is strongly dependent on the specific SFR (SFR/M_{star}) (Grimm et al. 2002; Gilfanov 2004). Using the SFR of $\sim 2.5\ M_\odot\ \mathrm{yr}^{-1}$ and the galaxy stellar mass of $\log M_\star/M_\odot = 10.3$, the specific SFR for J1224+5555 is approximately 2 times higher than that of the Milky Way (Grimm et al. 2002). For this specific SFR, HMXBs are expected to outnumber LMXBs at the highest luminosities by a factor of 4 (Gilfanov 2004). If the X-ray luminosity of J1224+5555 is attributable solely to XRBs, the underlying host galaxy should be dominated by a young stellar population, when the population of HMXBs is expected to be high. Using the near-infrared spectrum of J1224+5555, we investigated the extinction-insensitive age of the stellar population within the central 500 pc to see whether it is consistent with a population of HMXBs. The *H* band is dominated by the presence of stellar absorption lines (see Rayner et al. 2009 for examples). The strongest feature within that wavelength range is the CO (6–3) transition at 1.6189 μm. The CO bandhead is present in late-type giant stars, as well as younger red supergiants. The depth of the bandhead is known to vary with age and metallicity, providing a way to constrain the ages of the stellar populations (e.g., Oliva et al. 1995; Origilia et al. 1997, 1998). We used the Maraston & Strömbäck (2011, hereafter M11) set of intermediate- to high-resolution stellar population models, which include empirical stellar spectra. At the near-IR wavelengths of interest, the population models are sampled at 5 Å resolution, similar to the LUCI-1 data. The M11 near-IR models use the Pickles empirical library (Pickles 1998), which covers a broad range of evolutionary phases from O-type stars and supergiants to M dwarfs. We convolved the M11 models to match the instrumental resolution of the LUCI-1 observations. Then the CO (6–3) bandhead was measured in both the M11 models and LUCI-1 data using the prescribed definition and methodology from Origilia et al. (1998). Currently, M11 employ solar metallicity and include Kroupa, Chabrier, and Salpeter initial mass functions. In Figure 4, we plot the equivalent widths (EWs) of the CO bandhead for the three different M11 instantaneous starburst models as a function of time. The horizontal line is the measured EW of SDSS J1224+5555. As can be seen, the evolution of the CO (6–3) bandhead is age degenerate, since the red supergiant phase ($t < 20$ Myr) and red giant phase ($t > 300$ Myr) show a marked increase in the EWs. The measured EW of SDSS J1224+5555 intersects several points in the temporal evolution of the models. A commonly employed method to break this degeneracy is to use recombination emission lines to constrain the ages. The EWs of the recombination lines are strongly dependent on age, showing a steep decline as the most massive stars evolve off the main sequence. We applied the Starburst 99 (SB99) star formation models to the spectra of SDSS J1224+5555 (Leitherer et al. 1995, 2014). In Figure 4, we show the upper limit to the Brγ EW for J1224+5555. The near-infrared

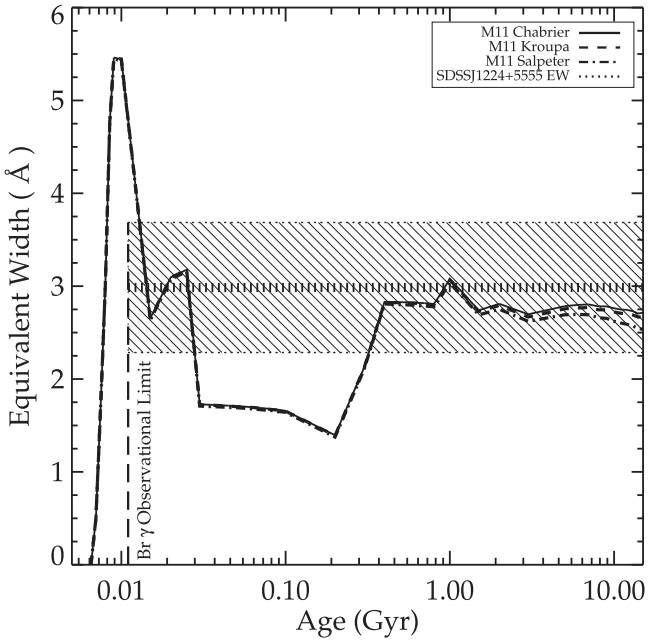

Figure 4. CO EW vs. age. The horizontal dashed line is the measured EW of CO(6–3), and the dotted gray lines above and below (and the diagonal hatched lines) indicate the EW error. The upper limit to the Brγ EW is indicated by the dashed vertical line. These two constraints imply a stellar population age greater than ~10 Myr.

[14] The National Radio Astronomy Observatory is a facility of the National Science Foundation operated under cooperative agreement by Associated Universities, Inc.

[15] http://sundog.stsci.edu/

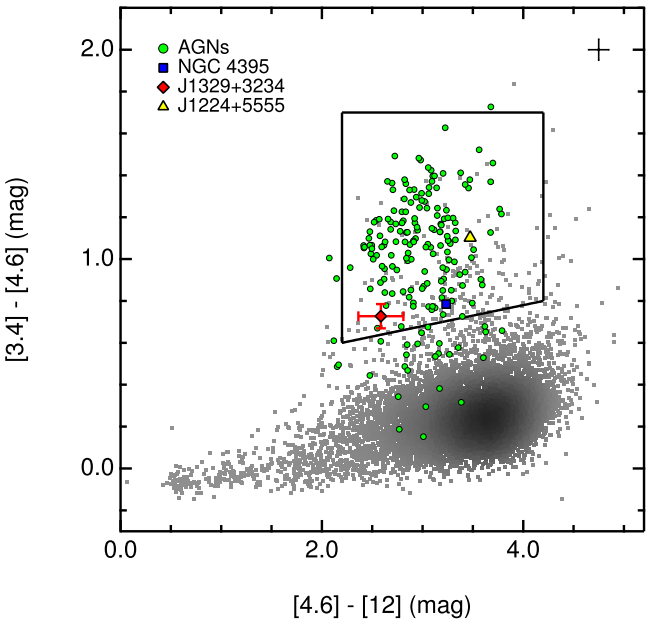

Figure 5. *W*1–*W*2 color vs. *W*2–*W*3 color for AGNs, optically star-forming galaxies from SDSS (gray dots), and J1224+5555, with J1329+3234 from Secrest et al. (2015b) and NGC 4395 included for comparison. The AGN region from Jarrett et al. (2011) is also shown as the solid polygon region, and the typical uncertainty for the AGN colors is given by the black cross at the top right.

spectrum therefore suggests that the underlying stellar population of the nuclear region in J1224+5555 is older than 10 Myr. For solar-metallicity galaxies, the peak in the number of bright HMXBs ($L_X > 10^{36}$ erg s^{-1}) is approximately 5 Myr after the burst (see Figure 1 in Linden et al. 2010), decreasing to below one HMXB for a starburst of $10^6\ M_\odot$. While the age implied by the near-infrared spectrum of J1224+5555 is not consistent with the peak in the HMXB population, we cannot rule out the possibility that the X-ray emission can be produced by a small number of extremely luminous HMXBs.

5. THE ORIGIN OF THE MID-INFRARED EMISSION

While the X-ray observation alone does not require the presence of an AGN, the mid-infrared emission from J1224+5555 is consistent with an AGN that dominates the mid-infrared luminosity. In Figure 5, we plot the *W*1–*W*2 versus *W*2–*W*3 colors of J1224+5555 together with the three-band AGN demarcation region from Jarrett et al. (2011). We also plot the mid-infrared colors of NGC 4395 and J1329+3234 from Secrest et al. (2015b), the hard X-ray selected sample of 184 AGNs from Secrest et al. (2015b), and galaxies classified as optically normal from the SDSS Data Release Eight. Optical emission line ratios were taken from the MPA/JHU DR8 catalogs,[16] and optically nonactive galaxies were identified using the demarcation between AGNs and star-forming galaxies from Stasinska et al. (2006). As can be seen, J1224+5555 falls squarely in the center of the AGN region and is significantly redder than J1329+3234 and the unambiguous broad-line AGN NGC 4395.

For samples of *known* AGNs, *WISE* color selection has been shown to be extremely reliable for identifying AGNs. For example, Stern et al. (2012) show that for a sample of *Spitzer*-identified AGNs from the *Spitzer*-COSMOS field (Sanders et al. 2007), a simple one-color *WISE* color cut of $W1–W2 > 0.8$ identifies AGNs with a reliability of 95%, and the two-color *WISE* selection criterion of Mateos et al. (2012) recovers luminous ($L_{2-10\,\mathrm{keV}} > 10^{44}$ erg s^{-1}) hard X-ray selected type 1 AGNs with a reliability of 97%. This same two-color selection criterion was also shown to by itself recover 98% of AGNs in a magnitude-limited ($g < 20$) sample from the SDSS-DR12Q catalog below a redshift of $z < 2$ (Secrest et al. 2015a). Thus, it is clear that for powerful AGNs, mid-infrared color selection is very effective in identifying AGNs.

We note that of all the optically classified SDSS galaxies plotted in Figure 5, only 1.8% have mid-infrared colors within the AGN demarcation region shown in Figure 5, demonstrating that mid-infrared colors of optically normal galaxies are rarely within the mid-IR AGN box. We also note that the absence of optical signatures of activity in these galaxies does not of course rule out the presence of an AGN. We searched the 3XMM-DR5 catalog (Rosen et al. 2016), which contains X-ray source detections drawn from 7781 *XMM-Newton* EPIC observations, to see if any of the optically normal galaxies in the mid-IR AGN box in Figure 5 have associated X-ray point sources. To guard against any potential bias that might be introduced by pointed observations of the targets, we conservatively selected only sources that were greater than 1′ from the *XMM-Newton* aim point to ensure that any detected point sources would be serendipitous discoveries. There are 132 optically normal star-forming galaxies in the mid-IR selection box plotted in Figure 5 that have X-ray sources in the 3XMM-DR5 catalog, 94% of which have $\log L_{2-10\,\mathrm{keV}} > 42$ erg s^{-1}, strongly suggesting that they host optically hidden AGNs. Thus, the sources inside the mid-infrared color selection region are overwhelmingly AGNs, and the mid-infrared colors of J1224+5555 are therefore highly suggestive of an AGN.

While the red mid-infrared color of J1224+5555 is highly suggestive of AGN activity, it is of course possible that red mid-infrared colors arise from dust heated by stellar processes. There have been a handful of low-metallicity BCDs with extreme red mid-infrared colors, raising the possibility that there is a similar origin for the hot dust in J1224+5555. For example, Izotov et al. (2011) find, from a sample of ∼5000 SDSS galaxies with *WISE* colors, four dwarf galaxies with extreme *WISE* colors ($W1–W2 > 2$ mag). Since the hardness of the stellar radiation increases with decreasing metallicity (e.g., Campbell et al. 1986), and BCDs contain significant star formation, the dust in BCDs can potentially be heated to higher temperatures than is typically seen in starburst galaxies. However, J1224+5555 has an above solar metallicity, suggesting that metallicity does not play a role in explaining the mid-infrared colors. Moreover, the four galaxies from the Izotov et al. (2011) sample occupy a separate region in mid-IR color space than J1224+5555, with much redder colors ($W1–W2 = 2.13–2.37$; $W2–W3 = 3.58–4.76$), indicating considerably more emission at longer wavelengths from dust heating due to starbursts. We also point out that the analysis of the EW of the CO bandhead and the absence of the Brγ line discussed in Section 4 suggests that the underlying nuclear stellar population in J1224+5555 is older than 10 Myr and therefore not consistent with the hottest dust that can be produced by star formation alone.

[16] https://www.sdss3.org/dr10/spectro/galaxy_mpajhu.php/

Figure 5 is suggestive that the mid-infrared emission is dominated by an AGN that is obscured in the optical. An excess in the mid-infrared emission expected from star formation is also suggested by the far-infrared emission from J1224+5555. If we assume that the galaxy's far-infrared emission is produced by stars alone and that even if the galaxy does host an AGN, its contribution to this wavelength range is negligible (de Grijp et al. 1985, 1987; Alton et al. 1998; Coziol et al. 1998; Netzer et al. 2007; Mullaney et al. 2011; Rosario et al. 2012), we predicted the *W2* luminosity expected from star formation assuming that it has a similar SED to the prototypical starburst, M82. The *W2*-to-60 μm flux ratio for M82 is $f_{\lambda,W2}/f_{\lambda,I60} = 0.54$ (Polletta et al. 2007), four times lower than the flux ratio in J1224+5555 ($f_{\lambda,W2}/f_{\lambda,I60} = 2.24 \pm 0.20$), strongly suggesting that most of the emission in the *W2* band is unlikely to be due to star formation and is most likely due to an obscured AGN. We note that the recent work by Ellison et al. (2016) using the *Herschel* data shows that the *IRAS*-derived far-infrared luminosities are overestimated in galaxies when a companion galaxy is nearby, as is the case for J1224+5555. Using the *Herschel* data as a training set, they employ artificial neural networks (ANNs) to generate a large public catalog of the far-infrared luminosities of a large sample of galaxies. The ANN value for the far-infrared luminosity from the Ellison et al. (2016) catalog is a factor of 2 lower than that predicted by *IRAS*, suggesting that the 60 μm flux from *IRAS* could be overestimated by a factor of 2, possibly suggesting an even larger discrepancy in the *W2*-to-60 μm flux ratio of a factor of 8 compared with M82.

Although the mid-infrared color of J1224+5555 is typical of dominant AGNs, its X-ray luminosity derived assuming only Galactic absorption is low compared to the hard X-ray selected sample of AGNs from Secrest et al. (2015b), the majority of which have $N_{\rm H} < 10^{22}\,{\rm cm}^{-2}$, which is in the range $\log L_{2-10\,{\rm keV}} = 42.1 - 46.7$ erg s^{-1}. The mid-infrared luminosity, thought to be re-emitted by the obscuring torus, and the AGN intrinsic 2–10 keV are known to follow a tight correlation over several orders of magnitude (Lutz et al. 2004; Gandhi et al. 2009; Mateos et al. 2015). In Figure 6, we plot the 6 μm band luminosity versus the observed hard X-ray luminosity for the AGN sample described in Secrest et al. (2015b), J1224+5555, and the Compton-thick sources for which *XMM-Newton* observations are available from the 70-month *Swift/BAT* catalog from Ricci et al. (2015). We also plot the effect of absorption on the local AGN relation using the MYTorus (Murphy & Yaqoob 2009) model assuming $\Gamma = 1.8$ and an inclination angle of $\theta = 90°$ with X-ray scattering fractions that ranged from 0.01% to 1% (dotted gray lines). As can be seen, J1224+5555 is significantly underluminous in the X-rays given its 6 μm luminosity compared with the AGN sample from Secrest et al. (2015b) and, like the sources from Ricci et al. (2015), is located near the Compton-thick regime. If we assume that the X-ray emission and 6 μm emission from J1224+5555 are due to an AGN, this suggests that the AGN is highly obscured, even in the X-rays. Using the linear regression fit between $L_{2-10\,{\rm keV}}$ and $L_{6\ \mu{\rm m}}$ for the AGN from Mateos et al. (2015) (green dashed line in Figure 6), and assuming an AGN power-law slope of $\Gamma = 1.8$, we estimate that the X-ray emitter in J1224+5555 is bordering on being Compton thick, with $N_{\rm H} \approx 3 \times 10^{24}\,{\rm cm}^{-2}$. For $N_{\rm H} \approx 10^{24}\,{\rm cm}^{-2}$, the unabsorbed hard X-ray luminosity is $L_{2-10\,{\rm keV}} \sim 3 \times 10^{42}$ erg s^{-1}. We note that the value of $N_{\rm H}$ adopted must be viewed with some caution since it depends on the X-ray model assumed and does not include an extinction correction to the 6 μm band luminosity, which may be significant for some Compton-thick sources (e.g., Goulding et al. 2012). Furthermore, we are assuming that the suppression of X-ray emission relative to the mid-infrared emission in J1224+5555 is due entirely to absorption and not intrinsic X-ray weakness, and that the contribution from star formation in the two bands is negligible. However, if there is an AGN in J1224+5555, it is likely that it is Compton thick with $N_{\rm H} > 10^{24}\,{\rm cm}^{-2}$. We adopt a value of $N_{\rm H} \approx 2 \times 10^{24}\,{\rm cm}^{-2}$ in this work.

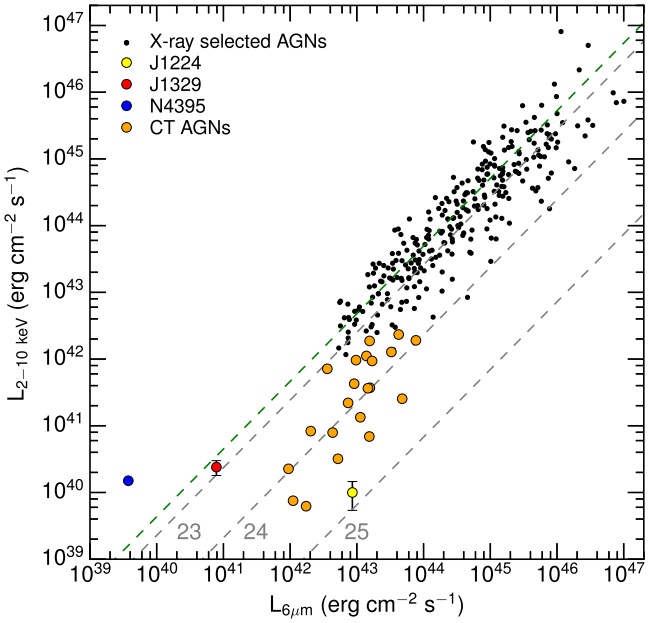

Figure 6. Observed 2–10 keV luminosity vs. the 6 μm luminosity for the hard X-ray selected sample of AGNs from Secrest et al. (2015b), J1224+5555, and the Compton-thick sources for which *XMM-Newton* observations are available from Ricci et al. (2015). For comparison, we also plot NGC 4395, the archetypical bulgeless dwarf Seyfert 1 galaxy, as well as J1329+3234, a bulgeless dwarf galaxy from Secrest et al. (2015b) that likely contains a massive black hole. The dashed green line shows the linear regression between $L_{6\ \mu\rm m}$ and intrinsic $L_{2-10\ \rm kev}$ from Mateos et al. (2015). The distance below this line is used to plot the median predicted relation assuming an intrinsic absorption of $N_{\rm H} = 1 \times 10^{22}\,{\rm cm}^{-2}$, $1 \times 10^{23}\,{\rm cm}^{-2}$, $1 \times 10^{24}\,{\rm cm}^{-2}$, and $1 \times 10^{25}\,{\rm cm}^{-2}$ using a MYTorus model assuming $\Gamma = 1.8$ and an inclination angle of $\theta = 90°$ with X-ray scattering fractions that ranged from 0.01% to 1% (gray dashed lines, with the exponent in the intrinsic $N_{\rm H}$ indicated at the base of each line).

6. THE ORIGIN OF THE NEAR-INFRARED EMISSION

The near-infrared spectral region offers access to several collisionally excited forbidden transitions in highly ionized species, a robust indicator of an AGN, and since the extinction in the *K* band is roughly a factor of 10 less than that in the optical, near-infrared spectroscopy potentially offers a less obscured view of the nuclear region. In addition, near-infrared broad hydrogen recombination lines can also reveal an optically hidden AGN. The LUCI-1 spectrum covers the wavelength of the [Si VI] 1.963 μm coronal line; however, no line was detected in the observed spectrum of J1224+5555. The absence of this line, however, is not unusual. Indeed, this line is frequently not detected even in optically confirmed type 2 AGNs (e.g., Riffel et al. 2006; Mason et al. 2015). Even

among a subsample of the *Swift*/BAT AGNs from the 70-month survey (Baumgartner et al. 2013), which represent the most powerful hard X-ray selected AGNs in the local universe, only ≈40% have detections in the [Si VI] line in recent follow-up observations (M. Koss et al. 2016, in preparation). If the extinction toward the AGN in J1224+5555 is very high, as the combined X-ray and mid-IR emission suggests, the absence of the [Si VI] 1.963 μm would therefore be expected.

Similarly, there is no evidence for a broad Paα or Brγ line in J1224+5555. However, the absence of broad recombination lines in the near-infrared is actually common even in optically identified type 2 AGNs. In a recent near-infrared spectroscopic study of local *Swift*/BAT AGNs with $42 < \log(L_{2-10\,\mathrm{keV}}) < 45\,\mathrm{erg\,s^{-1}}$, F. Onori et al. (2016, in preparation) find that only 14 out of 41 type 2 AGNs show broad Paβ emission. If the extinction toward the AGN in J1224+5555 is very high, the absence of the broad recombination lines in the near-infrared spectrum would therefore be expected.

Although the near-infrared spectrum of J1224+5555 does not show robust signatures of an AGN, we detected the H_2 $1-0S(3)$ 1.957 μm and H_2 $1-0S(3)$ 2.121 μm lines in the LUCI-1 spectrum. These lines are detected frequently in both star-forming and active galaxies with varying degrees of nuclear activity (e.g., Mouri 1994; Rodríguez-Ardila et al. 2004, 2005; Riffel et al. 2006, 2013; Mason et al. 2015). While there are multiple excitation mechanisms that can produce the emission lines, including UV fluorescence (Black & van Dishoeck 1987), shocks (Hollenbach & McKee 1989), and X-ray illumination (Maloney et al. 1996), each of which will produce a different H_2 emission line spectrum, there is considerable ambiguity in determining the dominant excitation mechanism responsible for the line emission. Moreover, the same excitation mechanisms may be at play in both star-forming galaxies and AGNs. However, empirically there appears to be a separation between AGNs and star-forming galaxies in the ratio of the near-infrared H_2 lines to the hydrogen recombination lines. In particular, several authors have noted a correlation between the [Fe II] 1.257 μm/Paβ and the H_2 $1-0\,S(1)$/Brγ ratio in galaxies, with the lowest ratios seen in star-forming galaxies (Larkin et al. 1998; Rodríguez-Ardila et al. 2005; Riffel et al. 2013). Using the largest sample of active and star-forming galaxies from Riffel et al. (2013), the line ratios are found to be separated by nuclear activity class according to the following demarcations: [Fe II]/Paβ < 0.6 and H_2/Brγ < 0.4 for star-forming galaxies; 0.6 < [Fe II]/Paβ < 2 and 0.4 < H_2/Brγ < 6 for AGNs; and for LINERs, [Fe II]/Paβ > 2 and H_2/Br γ > 6. Using the flux of the H_2 $1-0\,S(1)$ line and the upper limit to the Brγ flux, the H_2 $1-0\,S(1)$/Brγ flux ratio of J1224+5555 is >1.35, greater than the region generally occupied by star-forming galaxies. This raises the possibility that the extended emission probed by the [Fe II] and H_2 emission is influenced by the AGN, even though the broad line is obscured in the near-infrared. However, we point out that there is some overlap in these line ratios between the AGN and star-forming regions in the sample studied by Riffel et al. (2013), indicating that the interpretation of the emission lines ratios from such low ionization species is ambiguous (see also Smith et al. 2014).

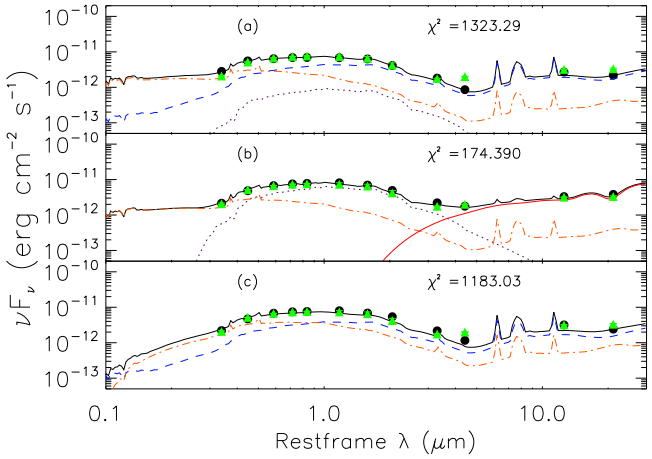

Figure 7. Observed photometry of SDSS J1224+5555 (green triangles) compared to model photometry (black circles, solid black line) created using combinations of the E (purple dotted line), Sbc (blue dashed line), Im (orange dot-dashed line), and AGN (red triple-dot-dashed line) templates from Assef et al. (2010). (a) Best-fit model of a linear combination of the E, Sbc, and Im templates assuming no additional extinction toward the galaxy templates. (b) Best-fit model using both the galaxy and AGN templates with variable extinction added to all the templates. (c) Best-fit model using only the galaxy templates but with additional extinction added as a free parameter. The χ^2 value for the fit is shown in the upper right of each plot.

7. MULTIWAVELENGTH SED

The multiwavength UV to mid-IR SED of J1224+5555 supports the scenario of a highly obscured AGN, based on the empirically derived templates of Assef et al. (2010). These templates consist of a set of three galaxy templates and one AGN template. The galaxy templates, E, Sbc, and Im, are based on templates from Coleman et al. (1980) with wavelength ranges extended using stellar models from Bruzual & Charlot (2003) and added dust and polycyclic aromatic hydrocarbon components from Devriendt et al. (1999). The AGN template is based on the average type 1 AGN template from Richards et al. (2006) with efforts to remove host galaxy contamination and create a template for an unobscured AGN. This method has since been used to successfully uncover highly obscured and even Compton-thick AGNs in several other works thus far (Chung et al. 2014; Hainline et al. 2014; Lansbury et al. 2014; Stern et al. 2014; Assef et al. 2015; Chen et al. 2015; Lansbury et al. 2015). Figure 7 shows the best-fit linear combination of the three galaxy templates to the observed SDSS, Two Micron All Sky Survey (2MASS), and *WISE* photometry of the target galaxy, where the best fit is obtained through a χ^2 minimization. The multiwavelength fluxes were obtained from the NASA/IPAC Extragalactic Database (NED).[17] The maximum wavelength of the Assef et al. (2010) templates is 30 μm; therefore, we cannot use the *IRAS* 60 μm flux in our fits. As discussed in Section 5, the 60 μm flux for J1224+5555 is likely overestimated, and its use is in any case questionable. While the SDSS g–z, 2MASS $J-K_s$, and *WISE* $W1$ bands are well fit by a combination of the Sbc and Im templates, the combined model flux is much lower than the observed fluxes in the $W2$–$W4$ bands. In fact, Table 2 of Assef et al. (2010) shows that at $z=0$ and $z=0.1$ no galaxy template has a $W1$–$W2$ color greater than 0.2 (Vega). However, when we add in the AGN template with a variable level of obscuration (red line) in

[17] https://ned.ipac.caltech.edu/

Figure 7, we see that the observed multiwavelength photometry of the galaxy is better fit with a combination of a young and old stellar population and highly obscured AGNs (red line) dominating the *WISE* bands, with a χ^2 value almost a factor of 7 times lower than the best fit obtained using the galaxy templates alone. As an additional test, we investigated the effect of adding variable additional extinction to the galaxy templates alone to determine if a comparable fit can be obtained without invoking the presence of an obscured AGN contribution. However, as can be seen from Figure 7, the best-fit model cannot adequately fit the SED in the *WISE* bands and results in a χ^2 value that is significantly worse than the model that includes an AGN (Figure 7). We note that the improvement in fit when the AGN template is added cannot be attributed simply to having additional model parameters in the fit. In the first model without an AGN, we achieve a χ^2 of 1323.29, with three model parameters. While the addition of an AGN template more than doubles the number of model parameters to 8, χ^2 is reduced by a factor of ~8, indicating that a model that includes an AGN template produces a significant improvement to the fit of the data.

We note that SED fitting of the multiwavelength photometry of galaxies can be highly degenerate. Furthermore, the Assef et al. (2010) templates are based on the median SEDs of large samples of galaxies. They therefore may not be appropriate to use on rare objects such as J1224+5555. Thus, while the above fits are suggestive of the presence of an obscured AGN, we do not consider them as providing robust proof of one.

8. DISCUSSION

The analysis of J1224+5555 conducted in this work reveals (1) an unresolved nuclear X-ray source consistent with but not exclusive to an AGN; (2) a near-infrared spectrum that suggests that the age of the underlying nuclear stellar population is beyond the peak of the HMXB population, suggesting that it is unlikely that the X-ray emission is produced by HMXBs; (3) a nuclear stellar population age that is not consistent with heating the dust to the highest temperatures possible from star formation alone; (4) possible evidence that the extended gas traced by the [Fe II] and H_2 near-infrared emission lines is influenced by an AGN; (5) no evidence for significant deeply embedded star formation based on an analysis of the near-infrared and optical recombination line ratios and the far-infrared and millimeter observations; (6) mid-infrared colors consistent with an AGN that dominates the mid-infrared luminosity; (7) an excess in the mid-infrared luminosity relative to the far-infrared luminosity, suggesting excess emission at mid-infrared wavelengths compared with that expected from star formation alone; and (8) a multi-wavelength SED that cannot be well fit by galaxy templates alone without the inclusion of an obscured AGN. While no one observation provides robust evidence for an AGN, the collective set of observations and analysis carried out in this paper suggests that J1224+5555 harbors a highly absorbed AGN.

8.1. Properties of the Putative AGN in J1224+5555

If we assume that a highly absorbed AGN resides in J1224+5555, we can estimate the black hole mass values for different accretion rate scenarios. If we assume that the source is nearly Compton thick ($N_H \approx 10^{24}$ cm^{-2}), the intrinsic hard X-ray luminosity is $L_{2-10\,keV} \sim 3 \times 10^{42}$ erg s^{-1}. Work from Vasudevan & Fabian (2009) has shown that the bolometric correction factor, $\kappa_{2-10\,keV}$, is a function of the Eddington rate. If we assume that J1224+5555 is a highly accreting AGN ($\lambda_{Edd} \sim 1$), the predicted bolometric correction factor is $\kappa_{2-10\,keV} = 100$, which yields a bolometric luminosity of the AGN of $L_{bol.} \sim 3 \times 10^{44}$ erg s^{-1} and an estimated black hole mass of $M_{BH} \simeq 2 \times 10^6\ M_\odot$. If instead we assume that J1224+5555 is in the low accreting regime ($\lambda_{Edd} \sim 0.02$), the predicted bolometric correction factor is $\kappa_{2-10\,keV} = 20$, which yields a bolometric luminosity of the AGN of $L_{bol.} \sim 6 \times 10^{43}$ erg s^{-1} and an estimated black hole mass of $M_{BH} \simeq 2 \times 10^7\ M_\odot$. In either scenario, J1224+5555 harbors a black hole of significant mass, well above the bulk of the distribution of plausible seed SMBH masses.

8.2. Obscured AGNs in Bulgeless Galaxies?

The discovery of a growing number of optically quiescent galaxies in the low-luminosity and low bulge mass regime with possible signatures of AGNs at X-ray and infrared wavelengths suggests that there may be an unexplored and significant population of obscured AGNs in the low-luminosity regime, and that the impact on discriminating between seed formation scenarios may be significant. It is well known that the shape and the intensity of the cosmic X-ray background cannot be reproduced successfully unless AGNs with intrinsic absorption of $N_H > 10^{24}$ cm^{-2} are a non-negligible fraction of the local AGN population (e.g., Comastri et al. 1995; Gilli et al. 2007; Treister et al. 2009). However, this population has been elusive in observational surveys, since identifying extremely obscured sources is challenging even in the local universe. Indeed, despite decades of multiwavelength observations from the X-ray to far-infrared wavelength region of the nearby ULIRG Arp 220, it is only through recent ALMA observations that an AGN obscured by a column density of $N_H = (0.6\text{–}1.8) \times 10^{25}$ cm^{-2} (Wilson et al. 2014; Scoville et al. 2015) has been confirmed.

In galaxies that lack signatures of an AGN in their optical spectrum, X-ray observations have been very successful in identifying obscured AGNs. However, at large column densities ($N_H > 10^{23}$ cm^{-2}), the observed 2–10 keV luminosity is significantly affected by absorption. Since the AGN intrinsic $L_{2-10\,keV}$ and the mid-infrared luminosity of the obscuring torus are known to follow a tight correlation over several orders of magnitude (Lutz et al. 2004; Gandhi et al. 2009; Mateos et al. 2015; Stern 2015), and the mid-infrared luminosity is less sensitive to obscuration, the selection of AGNs with very low X-ray to mid-infrared luminosity ratios has been used extensively to identify highly absorbed sources. Unlike J1329+3234, which appears to be only a moderately obscured AGN in a bulgeless dwarf galaxy, J1224+5555 shows signatures of heavier absorption. While we have only obtained two follow-up *XMM-Newton* observations of bulgeless galaxies from the sample from Satyapal et al. (2014), it is interesting to note that J1224+5555, which has a *W2* luminosity almost two orders of magnitude greater than that of J1329+3234, shows evidence for heavier absorption. Many studies suggest that the fraction of obscured AGNs relative to the whole population decreases at the lowest and highest luminosities (e.g., La Franca et al. 2005; Ballantyne et al. 2006; Treister & Urry 2006; Della Ceca et al. 2008; Winter et al. 2009; Brusa et al. 2010; Burlon et al. 2011). At high

luminosities, this is often attributed to a receding torus model (Lawrence 1991), in which the inner radius of the torus is set by the dust sublimation radius, which increases with AGN luminosity, a direct consequence of which would be an anticorrelation between the obscured AGN fraction and luminosity at high luminosities. On the other hand, at low luminosities, the torus obscuration may disappear, possibly because the clouds are generated by a disk-wind outflow, rather than accreted from the galaxy (Krolik & Begelman 1988), resulting in less absorption of the X-rays. If we can increase the sample of bulgeless galaxies with both mid-infrared and X-ray observations, we can gain a better understanding of the column density distribution function and its dependence on luminosity and host galaxy properties in AGNs in the local universe.

8.3. Challenges in Confirming AGNs in the Low-luminosity Regime—a Cautionary Tale

The combined analysis of the X-ray, mid-infrared, and near-infrared emission and the multiwavelength SED of J1224+5555 may suggest the presence of an obscured AGN, but definitive proof remains elusive. The detection of AGNs in this low-luminosity regime is challenging both because star formation in the host galaxy can dominate the optical spectrum and because gas and dust can obscure the central engine at both optical and X-ray wavelengths. For example, the detection of a compact radio source (Reines & Deller 2012) coincident with a moderately absorbed and variable nuclear X-ray point source (Reines et al. 2011; Whalen et al. 2015) in He 2–10 is highly suggestive of an AGN, despite its lack of AGN signatures in the optical. But the absorption-corrected 2–10 keV X-ray luminosity observed by *Chandra* is a factor of ≈ 4 lower than the observed 2–10 keV luminosity of J1224+5555, and the *WISE* colors of He 2–10 ($W1-W2 = 0.423$; $W2-W3 = 4.93$) are typical of starburst galaxies (see Figure 26 in Jarrett et al. 2011), suggesting that the AGN does not dominate in the infrared. Interestingly, He 2–10 shows no evidence for the high-ionization [Ne v] line in archival observations obtained with the high-resolution spectrograph on board *Spitzer*, and the ratio of the [Ne iii]/[Ne ii] line flux ratio, which is sensitive to the hardness of the radiation field, is a factor of ~10 lower than the average value in nearby starbursts (Engelbracht et al. 2008), suggesting that the putative AGN contributes minimally to the total bolometric luminosity of the galaxy. Thus, while mid-infrared color selection and X-ray observations at energies <10 keV are often powerful tools in uncovering optically obscured AGNs at higher luminosities, this is not the case in the low-luminosity regime. Indeed, none of the late-type and bulgeless galaxies that show evidence for the high-excitation [Ne v] line, a robust indicator of AGN activity, (Satyapal et al. 2007, 2008, 2009), would be selected as AGNs based on optical spectroscopy or mid-infrared color selection by *WISE*.

Similarly, as demonstrated in this work, the X-ray luminosities of weak AGNs will be low and can be comparable to, and therefore indistinguishable from, XRBs in the host galaxy. We should note that while several works have attempted to correct for the X-ray emission expected from XRBs, there is considerable scatter in the relation, and there are numerous relations that have been derived using different samples of galaxies (e.g., Grimm et al. 2003; Ranalli et al. 2003; Gilfanov et al. 2004; Lehmer et al. 2010; Mineo et al. 2012) that show that the stellar mass, SFR, stellar population age, and mean metallicity can significantly affect the X-ray output of a given XRB population (Fragos et al. 2013). Furthermore, the estimate of the nuclear SFR can vary significantly in different works, ranging from the use of optical or UV continuum measurements, to optical recombination line measurements, to *IRAS* fluxes, to SED fitting, introducing additional uncertainties. Thus, caution must be exercised in determining a true excess in the X-ray emission expected over stellar sources in the low–luminosity regime. Indeed, recent high spatial resolution integral field observations of the bulgeless galaxy NGC 3621 reveal that the narrow line emitting gas is spatially offset from the X-ray source previously identified as an AGN (Gliozzi et al. 2009), raising the possibility that the X-ray source is not associated with the AGN (Menezes et al. 2016).

These observations highlight the ambiguity associated with optical, X-ray, and mid-infrared color selection in the low-luminosity regime, where both star formation and obscuration can both be at play and responsible for hiding the AGN. Indeed, recent *NuSTAR* observations were required to provide definite proof of a low-luminosity AGN in the luminous infrared galaxy NGC 6286, demonstrating that both heavy obscuration and a weak AGN can hide the AGN signatures at optical, infrared, and lower-energy X-ray observations (Ricci et al. 2016). There are a growing number of such low-luminosity and optically unidentified AGNs that show evidence for heavy absorption based on *NuSTAR* observations (A. Annuar et al. 2016, in preparation). For very high absorption, it is even possible that mid-infrared selection can fail even in luminous AGNs, as has recently been found in several *Swift*/BAT AGNs (M. Koss et al. 2016, in preparation). Adding to the complexities described above, the time lag between the onset of accretion and its visibility at X-ray wavelengths and in the much more extended narrow line region gas can also result in an incomplete census of AGN activity. The impact of this effect is discussed recently by Schawinski et al. (2015) and may provide another explanation for the lack of optical signatures in some of the optically identified AGNs in the low bulge mass regime. We note that while radio observations are insensitive to obscuration, the radio emission in AGNs can be dominated by and indistinguishable from compact nuclear starbursts (Condon et al. 1991; Del Moro et al. 2013). Furthermore, only approximately 10% of AGNs are radio loud, and the radio-loud fraction for low-mass AGNs in particular is poorly known (Miller et al. 1990; Stern et al. 2000). Even broad emission lines in the optical spectrum, a robust indicator of an AGN for large black hole masses, is associated with star formation for the majority of cases in dwarf galaxies (Baldassare et al. 2015), further emphasizing the limitations of optical studies in finding AGNs in the low bulge mass regime.

What is the path forward in identifying AGNs in the low bulge mass regime? Based on the hunt for AGNs in the low bulge mass regime thus far, it is clear that multiwavelength observations are crucial in our attempt to arrive at a complete census, and that studies based on only one technique will be incomplete. Given that we now know that obscuration and host galaxy contamination are often both at play in the low-luminosity regime, a promising prospect will be sensitive mid-infrared spectroscopic observations of the [Ne v] emission line that will be enabled by the *James Webb Space Telescope*, which can robustly separate starbursts from AGNs (Abel & Satyapal 2008) and potentially yield as much as 4 times as

many AGNs in galaxies that lack classical bulges compared to optical studies (Satyapal et al. 2008).

9. SUMMARY AND CONCLUSIONS

We have conducted the second follow-up X-ray observation of a newly discovered population of bulgeless galaxies that display extremely red mid-infrared colors highly suggestive of a dominant AGN despite having no optical signatures of accretion activity. Our main results can be summarized as follows:

1. Using *XMM-Newton* observations, we have confirmed the presence of an unresolved X-ray source coincident with the nucleus of J1224+5555, an optically normal bulgeless galaxy with red infrared colors obtained from *WISE*.
2. The observed X-ray luminosity (uncorrected for intrinsic absorption) of J1224+5555 is $L_{2-10\,\mathrm{keV}} = (1.1 \pm 0.4) \times 10^{40}\,\mathrm{erg\,s^{-1}}$, which is a factor of 3–4 lower than the luminosity expected from XRBs in the host galaxy. But given the scatter in the relation, the observed X-ray luminosity is not significantly above the relation.
3. While the X-ray observations alone do not require the presence of an AGN, a multiwavelength investigation of the X-ray, near-IR, and mid-IR activity of J1224+5555 is consistent with the presence of a highly obscured and energetically dominant AGN with column density $N_{\mathrm{H}} > 10^{24}\,\mathrm{cm^{-2}}$.
4. The hard X-ray luminosity of the putative AGN corrected for absorption is $L_{2-10\,\mathrm{keV}} \sim 3 \times 10^{42}\,\mathrm{erg\,s^{-1}}$, which, depending on the bolometric correction factor, corresponds to a bolometric luminosity of the AGN of $L_{\mathrm{bol.}} \sim 6 \times 10^{43}\,\mathrm{erg\,s^{-1}} - 3 \times 10^{44}\,\mathrm{erg\,s^{-1}}$ and a lower mass limit for the black hole of $M_{\mathrm{BH}} \simeq 2 \times 10^{6}\,M_{\odot} - 2 \times 10^{7}\,M_{\odot}$, based on the Eddington limit.
5. There is no evidence for coronal lines or broad lines in the near-infrared spectrum of J1224+5555, suggesting that the putative AGN is obscured even in the *K* band.
6. These observations demonstrate the ambiguity associated with identifying AGNs in the low-luminosity regime and highlight the need for a careful mutliwavelength investigation.

The X-ray observations of J1224+5555 presented here are one of the two only follow-up observations of bulgeless galaxies with red mid-infrared colors discovered by *WISE*. Both targets point to the presence of optically obscured AGNs, suggesting that some low-mass and bulgeless galaxies do harbor AGNs. These observations may suggest that optically normal AGNs in bulgeless galaxies are more common than previously thought, and emphasize the need for more follow-up multiwavelength studies of this population.

We gratefully acknowledge the anonymous referee for a very thorough and insightful review that improved this manuscript. We also gratefully acknowledge very helpful discussions with Daniel Stern on the ambiguities associated with mid-infrared color selection in low-mass and bulgeless galaxies. The plots in this paper greatly benefited from previously written scripts by Paul McNulty, with whom it has been a joy to work. N.J.S. and S.S. gratefully acknowledge support by the *XMM* Guest Investigator Program under NASA Grant NNX14AF02G and a Mason 4-VA Innovation grant. J.L.R. and J.A.O. acknowledge support from NSF-AST 000167932. R.C.H. acknowledges support from an Alfred P. Sloan Research Fellowship and from the National Science Foundation through grant number 1515364. A.C. acknowledges support from the JMU 4-VA grant. N.J.S. acknowledges support from a National Research Council Associateship Award at the Naval Research Laboratory. Basic research in astronomy at the Naval Research Laboratory is funded by the Office of Naval Research. This research has made use of the NASA/IPAC Extragalactic Database (NED), which is operated by the Jet Propulsion Laboratory, California Institute of Technology, under contract with the National Auronautics and Space Administration. We also gratefully acknowledge the use of the software TOPCAT (Taylor 2005) and Astropy (Astropy Collaboration et al. 2013).

REFERENCES

Abel, N. P., & Satyapal, S. 2008, ApJ, 678, 686
Agarwal, B., Dalla Vecchia, C., Johnson, J. L., Khochfar, S., & Paardekooper, J.-P. 2014, MNRAS, 443, 648
Alton, P. B., Davies, J. I., & Trewhella, M. 1998, MNRAS, 296, 773
Alvarez, M. A., Wise, J. H., & Abel, T. 2009, ApJL, 701, L133
Araya Salvo, C., Mathur, S., Ghosh, H., Fiore, F., & Ferrarese, L. 2010, ApJ, 757, 179
Assef, R. J., Eisenhardt, P. R. M., Stern, D., et al. 2015, ApJ, 804, 27
Assef, R. J., Kochanek, C. S., Brodwin, M., et al. 2010, ApJ, 713, 970
Astropy Collaboration, Robitaille, T. P., Tollerud, E. J., et al. 2013, A&A, 558, A33
Baldassare, V. F., Reines, A. E., Gallo, E., et al. 2015, ApJL, 809, L14
Ballantyne, D. R., Shi, Y., Rieke, G. H., et al. 2006, ApJ, 653, 1070
Barth, A. J., Ho, L. C., Rutledge, R. E., & Sargent, W. L. W. 2004, ApJ, 607, 90
Baumgartner, W. H., Tueller, J., Markwardt, C. B., et al. 2013, ApJS, 207, 19
Begelman, M. C., & Rees, M. J. 1978, MNRAS, 185, 847
Bell, E. F. 2003, ApJ, 586, 794
Bizzocchi, L., Filho, M. E., Leonardo, E., et al. 2014, ApJ, 782, 22
Black, J. H., & van Dishoeck, E. F. 1987, ApJ, 322, 412
Brinchmann, J., Charlot, S., White, S. D. M., et al. 2004, MNRAS, 351, 1151
Bromm, V., & Loeb, A. 2003, ApJ, 596, 34
Brusa, M., Civano, F., Comastri, A., et al. 2010, ApJ, 716, 348
Bruzual, G., & Charlot, S. 2003, MNRAS, 344, 1000
Burlon, D., Ajello, M., Greiner, J., et al. 2011, ApJ, 728, 58
Campbell, A., Terlevich, R., & Melnick, J. 1986, MNRAS, 223, 811
Chen, C.-T. J., Hickox, R. C., Alberts, S., et al. 2015, ApJ, 802, 50
Chung, S. M., Kochanek, C. S., Assef, R., et al. 2014, ApJ, 790, 54
Coelho, B., Antón, S., Lobo, C., & Ribeiro, B. 2013, MNRAS, 436, 2426
Coleman, G. D., Wu, C. C., & Weedman, D. W. 1980, ApJS, 43, 393
Comastri, A., Setti, G., Zamorani, G., & Hasinger, G. 1995, A&A, 296, 1
Condon, J. J., Huang, Z.-P., Yin, Q. F., & Thuan, T. X. 1991, ApJ, 378, 65
Coziol, R., Torres, C. A. O., Quast, G. R., Contini, T., & Davoust, E. 1998, ApJS, 119, 239
de Grijp, M. H. K., Lub, J., & Miley, G. K. 1987, A&AS, 70, 95
de Grijp, M. H. K., Miley, G. K., Lub, J., & de Jong, T. 1985, Natur, 314, 240
Del Moro, A., Alexander, D. M., Mullaney, J. R., et al. 2013, A&A, 549, A59
Della Ceca, R., Caccianiga, A., Severgnini, P., et al. 2008, A&A, 487, 119
Desroches, L. B., & Ho, L. C. 2009, ApJ, 690, 267
Devriendt, J. E. G., Guiderdoni, B., & Sadat, R. 1999, A&A, 350, 381
Dewangan, G. C., Mathur, S., Griffiths, R. E., & Rao, A. R. 2008, ApJ, 689, 762
Dong, X.-B., Ho, L. C., Yuan, W., et al. 2012, ApJ, 755, 167
Ebisuzaki, T., Makino, J., Tsuru, T. G., et al. 2001, ApJL, 562, L19
Ellison, S. L., Teimoorinia, H., Rosario, D. J., & Mendel, J. T. 2016, MNRAS, 455, 370
Engelbracht, C. W., Rieke, G. H., Gordon, K. D., et al. 2008, ApJ, 678, 804
Fan, X., Strauss, M. A., Richards, G. T., et al. 2006, AJ, 131, 1203
Filippenko, A., & Ho, L. 2000, ApJL, 588, L13
Fragos, T., Lehmer, B. D., Naoz, S., Zezas, A., & Basu-Zych, A. 2013, ApJL, 776, L31
Gandhi, P., Horst, H., Smette, A., et al. 2009, A&A, 502, 457
Ghosh, H., Mathur, S., Fiore, F., & Ferrarese, L. 2008, AIPC, 1053, 39G
Gilfanov, M. 2004, MNRAS, 349, 146
Gilfanov, M., Grimm, H.-J., & Sunyaev, R. 2004, MNRAS, 347, L57

Gilli, R., Comastri, A., & Hasinger, G. 2007, A&A, 463, 79
Gliozzi, M., Satyapal, S., Erancleous, M., Titarchuk, L., & Cheung, C. C. 2009, ApJ, 700, 1759
Goulding, A. D., & Alexander, D. M. 2009, MNRAS, 398, 1165
Goulding, A. D., Alexander, D. M., Bauer, F. E., et al. 2012, ApJ, 755, 5
Graham, A. W., Ciambur, B. C., & Soria, R. 2016, ApJ, 818, 172
Graham, A. W., & Scott, N. 2015, ApJ, 798, 54
Greene, J. E. 2012, NatCo, 3, 1304
Greene, J. E., & Ho, L. C. 2007, ApJ, 667, 131
Greif, T. H., Springel, V., White, S. D. M., et al. 2011, ApJ, 737, 75
Griffith, R. L., et al. 2011, ApJL, 736, L22
Grimm, H.-J., Gilfanov, M., & Sunyaev, R. 2002, A&A, 391, 923
Grimm, H.-J., Gilfanov, M., & Sunyaev, R. 2003, MNRAS, 339, 793
Haehnelt, M. G., & Rees, M. J. 1993, MNRAS, 263, 168
Hainline, K. N., Hickox, R. C., Carroll, C. M., et al. 2014, ApJ, 795, 124
Ho, L. C., Kim, M., & Terashima, Y. 2012, ApJL, 759, L16
Hollenbach, D., & McKee, C. F. 1989, ApJ, 342, 306
Hopkins, P. F., Hickox, R., Quataert, E., & Hernquist, L. 2009, MNRAS, 398, 333
Hopkins, P. F., Kocevski, D. D., & Bundy, K. 2014, MNRAS, 445, 823
Izotov, Y. I., Guseva, N. G., Fricke, K. J., & Henkel, C. 2011, A&A, 536, L7
Izotov, Y. I., Guseva, N. G., Fricke, K. J., & Henkel, C. 2014, A&A, 561, A33
Izotov, Y. I., & Thuan, T. X. 2008, ApJ, 687, 133
Jarrett, T. H., Cohen, M., Masci, F., et al. 2011, ApJ, 735, 112
Jiang, Y.-F., Greene, J. E., Ho, L. C., Xiao, T., & Barth, A. J. 2011, ApJ, 742, 68
Johnson, J. L., & Bromm, V. 2007, MNRAS, 374, 1557
Kalberla, P. M. W., Burton, W. B., Hartmann, D., et al. 2005, A&A, 440, 775
Kauffmann, G., et al. 2003, MNRAS, 346, 1055
Kewley, L. J., Dopita, M. A., Sutherland, R. S., Heisler, C. A., & Trevena, J. 2001, ApJ, 556, 121
Krolik, J. H., & Begelman, M. C. 1988, ApJ, 329, 702
La Franca, F., Fiore, F., Comastri, A., et al. 2005, ApJ, 635, 864
Landini, M., Natta, A., Salinari, P., Oliva, E., & Moorwood, A. F. M. 1984, A&A, 134, 284
Lansbury, G. B., Alexander, D. M., Del Moro, A., et al. 2014, ApJ, 785, 17
Lansbury, G. B., Gandhi, P., Alexander, D. M., et al. 2015, arXiv:1506.05120
Larkin, J. E., Armus, L., Knop, R. A., Soifer, B. T., & Matthews, K. 1998, ApJS, 114, 59
Lawrence, A. 1991, MNRAS, 252, 586
Lehmer, B. D., Alexander, D. M., Bauer, F. E., et al. 2010, ApJ, 724, 559
Leitherer, C., Ekström, S., Meynet, G., et al. 2014, ApJS, 212, 14
Leitherer, C., et al. 1995, ApJS, 123, 3
Lemons, S. M., Reines, A. E., Plotkin, R. M., Gallo, E., & Greene, J. E. 2015, ApJ, 805, 12
Linden, T., Kalogera, V., Sepinsky, J. F., et al. 2010, ApJ, 725, 1984
Lutz, D., Maiolino, R., Spoon, H. W. W., & Moorwood, A. F. M. 2004, A&A, 418, 465
Maksym, W. P., Ulmer, M. P., Roth, K. C., et al. 2014, MNRAS, 444, 866
Maloney, P. R., Hollenbach, D. J., & Tielens, A. G. G. M. 1996, ApJ, 466, 561
Maraston, C., & Strömbäck, G. 2011, MNRAS, 418, 2785
Mason, R. E., Rodríguez-Ardila, A., Martins, L., et al. 2015, ApJS, 217, 13
Mateos, S., Alonso-Herrero, A., Carrera, F. J., et al. 2012, MNRAS, 426, 3271
Mateos, S., Carrera, F. J., Alonso-Herrero, A., et al. 2015, MNRAS, 449, 1422
McAlpine, W., Satyapal, S., Gliozzi, M., et al. 2010, ApJ, 728, 1
Menezes, R. B., Steiner, J. E., & da Silva, P. 2016, ApJ, 817, 150
Mezcua, M., Civano, F., Fabbiano, G., Miyaji, T., & Marchesi, S. 2016, ApJ, 817, 20
Miller, B. P., Gallo, E., Greene, J. E., et al. 2015, ApJ, 799, 98
Miller, L., Peacock, J. A., & Mead, A. R. G. 1990, MNRAS, 244, 207
Mineo, S., Gilfanov, M., & Sunyaev, R. 2012, MNRAS, 419, 2095
Moran, E. C., Shahinyan, K., Sugarman, H. R., Vélez, D. O., & Eracleous, M. 2014, AJ, 148, 136
Mortlock, D. J., Warren, S. J., Venemans, B. P., et al. 2011, Natur, 474, 616
Mouri, H. 1994, ApJ, 427, 777
Mullaney, J. R., Alexander, D. M., Goulding, A. D., & Hickox, R. C. 2011, MNRAS, 414, 1082
Murphy, K. D., & Yaqoob, T. 2009, MNRAS, 397, 1549
Natarajan, P. 2014, GReGr, 46, 1702
Netzer, H., Lutz, D., Schweitzer, M., et al. 2007, ApJ, 666, 806
Oliva, E., Origlia, L., Kotilaninen, J. K., & Moorwood, A. F. M. 1995, A&A, 301, 55
Origlia, L., Ferraro, F. R., Fusi Pecci, F., & Oliva, E. 1997, A&A, 321, 859
Origlia, L., Moorwood, A. F. M., & Oliva, E. 1998, A&A, 280, 536
Osterbrock, D. E., & Ferland, G. J. 2006, Astrophysics of Gaseous Nebulae and Active Galactic Nuclei (2nd ed.; Sausalito: Univ. Science Books)
Pickles, A. J. 1998, PASP, 110, 863
Polletta, M., Tajer, M., Maraschi, L., et al. 2007, ApJ, 663, 81
Pons, E., & Watson, M. G. 2014, A&A, 568, A108
Ranalli, P., Comastri, A., & Setti, G. 2003, A&A, 399, 39
Rayner, J. T., Cushing, M. C., & Vacca, W. D. 2009, ApJS, 185, 289
Regan, J. A., Johansson, P. H., & Haehnelt, M. G. 2014, MNRAS, 439, 1160
Reines, A. E., & Deller, A. T. 2012, ApJL, 750, L24
Reines, A. E., Greene, J. E., & Geha, M. 2013, ApJ, 775, 116
Reines, A. E., Plotkin, R. M., Russell, T. D., et al. 2014, ApJL, 787, L30
Reines, A. E., Sivakoff, G. R., Johnson, K. E., & Brogan, C. L. 2011, Natur, 470, 66
Ricci, C., Bauer, F. E., Treister, E., et al. 2016, arXiv:1601.05800
Ricci, C., Ueda, Y., Koss, M. J., et al. 2015, ApJL, 815, L13
Richards, G. T., Lacy, M., Storrie-Lombardi, L. J., et al. 2006, ApJS, 166, 470
Riffel, R., Rodríguez-Ardila, A., Aleman, I., et al. 2013, MNRAS, 430, 2002
Riffel, R., Rodríguez-Ardila, A., & Pastoriza, M. G. 2006, A&A, 457, 61
Rodríguez-Ardila, A., Pastoriza, M. G., Viegas, S., Sigut, T. A. A., & Pradhan, A. K. 2004, A&A, 425, 457
Rodríguez-Ardila, A., Riffel, R., & Pastoriza, M. G. 2005, MNRAS, 364, 1041
Rosario, D. J., Santini, P., Lutz, D., et al. 2012, A&A, 545, A45
Rosen, S. R., Webb, N. A., Watson, M. G., et al. 2016, A&A, 590, A1
Safranek-Shrader, C., Milosavljević, M., & Bromm, V. 2014, MNRAS, 440, L76
Salim, S., Rich, R. M., Charlot, S., et al. 2007, ApJS, 173, 267
Sanders, D. B., Salvato, M., Aussel, H., et al. 2007, ApJS, 172, 86
Sartori, L. F., Schawinski, K., Treister, E., et al. 2015, MNRAS, 454, 3722
Satyapal, S., Böker, T., Mcalpine, W., et al. 2009, ApJ, 704, 439
Satyapal, S., Secrest, N. J., McAlpine, W., et al. 2014, ApJ, 784, 113
Satyapal, S., Vega, D., Dudik, R. P., Abel, N. P., & Heckman, T. 2008, ApJ, 677, 926
Satyapal, S., Vega, D., Heckman, T., O'Halloran, B., & Dudik, R. 2007, ApJL, 663, L9
Schawinski, K., Koss, M., Berney, S., & Sartori, L. F. 2015, MNRAS, 451, 2517
Schramm, M., Silverman, J. D., Greene, J. E., et al. 2013, ApJ, 773, 150
Scoville, N., Sheth, K., Walter, F., et al. 2015, ApJ, 800, 70
Secrest, N. J., Dudik, R. P., Dorland, B. N., et al. 2015a, ApJS, 221, 12
Secrest, N. J., Satyapal, S., Gliozzi, M., et al. 2012, ApJ, 753, 38
Secrest, N. J., Satyapal, S., Gliozzi, M., et al. 2015b, ApJ, 798, 38
Secrest, N. J., Satyapal, S., Moran, S. M., et al. 2013, ApJ, 777, 139
Seifert, W., et al. 2003, Proc. SPIE, 4841, 962
Seifert, W., et al. 2010, Proc. SPIE, 7735, 7
Shields, J. C., et al. 2008, ApJ, 682, 104
Simmons, B. D., Lintott, C., Schawinski, K., et al. 2013, MNRAS, 429, 2199
Smith, K. L., Koss, M., & Mushotzky, R. F. 2014, ApJ, 794, 112
Stasinska, G., Cid Fernandes, R., Mateus, A., Sodre, L., & Asari, N. V. 2006, MNRAS, 371, 972
Stern, D. 2015, ApJ, 807, 129
Stern, D., Assef, R. J., Benford, D. J., et al. 2012, ApJ, 753, 30
Stern, D., Djorgovski, S. G., Perley, R. A., de Carvalho, R. R., & Wall, J. V. 2000, AJ, 119, 1526
Stern, D., Lansbury, G. B., Assef, R. J., et al. 2014, ApJ, 794, 102
Taylor, M. B. 2005, adass XIV, 347, 29
Treister, E., & Urry, C. M. 2006, ApJL, 652, L79
Treister, E., Urry, C. M., & Virani, S. 2009, ApJ, 696, 110
Tremonti, C. A., Heckman, T. M., Kauffmann, G., et al. 2004, ApJ, 613, 898
Trump, J. R., Sun, M., Zeimann, G. R., et al. 2015, ApJ, 811, 26
Vacca, W. D., Cushing, M. C., & Rayner, J. T. 2003, PASP, 115, 389
van Wassenhove, S., Volonteri, M., Walker, M. G., & Gair, J. R. 2010, MNRAS, 408, 1139
Vasudevan, R. V., & Fabian, A. C. 2009, MNRAS, 392, 1124
Venemans, B. P., Findlay, J. R., Sutherland, W. J., et al. 2013, ApJ, 779, 24
Volonteri, M. 2010, A&ARv, 18, 27
Volonteri, M., Haardt, F., & Madau, P. 2003, ApJ, 582, 559
Volonteri, M., & Natarajan, P. 2009, MNRAS, 400, 1911
Volonteri, M., & Rees, M. J. 2005, ApJ, 633, 624
Whalen, T. J., Hickox, R. C., Reines, A. E., et al. 2015, ApJ, 806, 37
Willingale, R., Starling, R. L. C., Beardmore, A. P., Tanvir, N. R., & O'Brien, P. T. 2013, MNRAS, 431, 394
Wilson, C. D., Rangwala, N., Glenn, J., et al. 2014, ApJL, 789, L36
Winter, L. M., Mushotzky, R. F., Reynolds, C. S., & Tueller, J. 2009, ApJ, 690, 1322
Wright, et al. 2010, AJ, 140, 1868
Wu, X.-B., Wang, F., Fan, X., et al. 2015, Natur, 518, 512
Yuan, W., Zhou, H., Dou, L., et al. 2014, ApJ, 782, 55